scientific reports

Check for updates

OPEN

# 1, 4-benzodioxan-substituted Thienyl chalcone derivatives as novel reversible inhibitors of human monoamine oxidase B with anti-neuroinflammatory activity

Demeng Sun, Mengxue Mu, Yanmei Jiang, Bo Wang, Zuo Kong, Jingbo Tan & Yun Hu✉

**In this study, a series of 1, 4-benzodioxan-substituted thienyl chalcone derivatives were designed, synthesized and evaluated for their inhibitory activities against human MAO-B (*h*MAO-B). The structure-activity relationship was investigated and summarized. Among the 22 derivatives, compound 12 showed the most potent inhibitory activity, which exhibited an $IC_{50}$ of 0.11 μM with a selectivity index greater than 333. Kinetics and reversibility studies confirmed that compound 12 acted as a competitive and reversible inhibitor of *h*MAO-B. Molecular docking studies revealed the enzyme-inhibitor interactions and the rationale was provided. Moreover, compound 12 could effectively inhibit the release of nitric oxide, tumor necrosis factor-alpha and interleukin-1 beta in both lipopolysaccharide and amyloid β-protein 1–42 ($Aβ_{1-42}$)-stimulated BV2 cells and attenuate the cytotoxicity induced by $Aβ_{1-42}$ in BV2 cells. As compound 12 exhibited low neurotoxicity, we believe the hit compound which combines the activities of MAO-B inhibiting and anti-neuroinflammation could be further investigated as a novel potential lead for future studies.**

**Keywords** Monoamine oxidase B inhibitors, Anti-neuroinflammation, 1, 4-benzodioxan, Chalcone

Oxidative stress and neuroinflammation are recognized as important contributors to the pathogenesis of neurodegenerative diseases, such as Parkinson's disease (PD) and Alzheimer's disease (AD)[1,2]. Evidence indicates that the flavin-dependent enzymes known as monoamine oxidases (MAOs) are closely associated with oxidative stress[3,4]. There are two isoforms of monoamine oxidases: MAO-A and MAO-B. MAO-A is primarily expressed in the intestinal mucosa and sympathetic nerve terminals, whereas MAO-B is predominant isoform in the brain of adults[5,6]. Generally, MAOs catalyze the oxidative deamination of monoamines, including the neurotransmitters dopamine and tyramine, during which hydrogen peroxide ($H_2O_2$) is produced[7]. In the brains of patients with PD and AD, both the expression and activity of MAO-B have been found to be significantly elevated, leading to a depletion of neurotransmitters and an increase in $H_2O_2$levels[8,9]. The excessive $H_2O_2$can be converted into highly neurotoxic hydroxyl radicals, thereby exacerbating oxidative stress in the brain. From this perspective, inhibiting MAO-B is expected to enhance the availability of neurotransmitters and reduce oxidative stress in the brains of patients with PD and AD. Thus, MAO-B inhibitors are considered as promising therapeutic agents for PD and AD[10].

There are two types of MAO-B inhibitors currently used in clinical practice (Fig. 1A). The first type is the irreversible inhibitors, including *R*-(-)-deprenyl and rasagiline, which could covalently bind to the enzyme. The second type is the reversible inhibitors, such as safinamide, which inhibit MAO-B through no-covalent interactions and typically have safer profiles[11].

Neuroinflammation is another important factor contributing to neurodegenerative diseases which involves the activation of microglia in the central nervous system[12]. Microglia can be activated by pathological stimuli such as lipopolysaccharide (LPS) and amyloid beta (Aβ) and release the pro-inflammatory mediators, including nitric oxide (NO), tumor necrosis factor-alpha (TNF-α), and interleukin-1 beta (IL-1β)[13,14]. Chronic neuroinflammatory responses can result in cellular damage and the loss of neuronal function. Therefore,

School of Bioengineering, Zunyi Medical University, Zhuhai Campus, Zhuhai 519041, China. ✉email: ce04hy@mail2.sysu.edu.cn

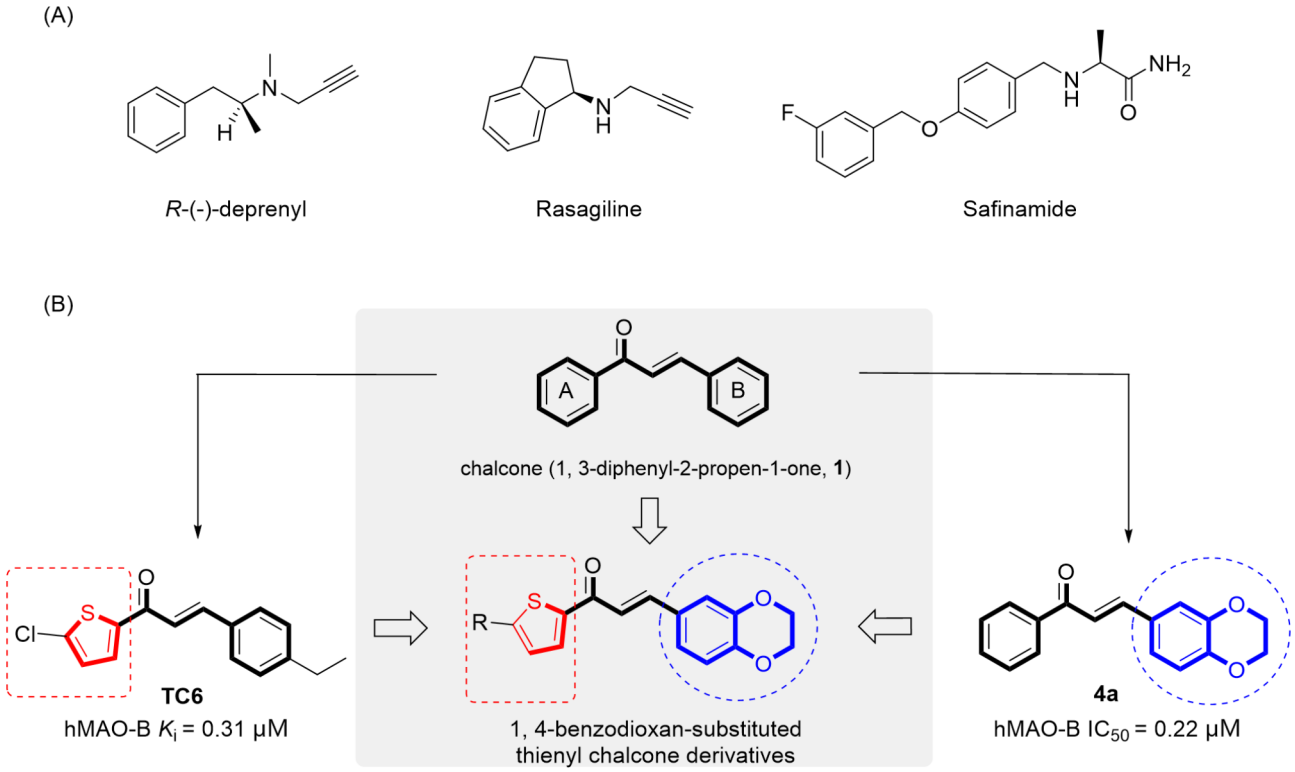


**Fig. 1**. Structures of irreversible and reversible MAO inhibitors in clinical use (**A**) and the potencies of previously described MAO-B inhibitors (**B**). Middle, the design strategy of 1, 4-benzodioxan -substituted thienyl chalcone compounds.

suppressing microglial activation is considered as another promising therapeutic strategy for neurodegenerative diseases[15].

In the search for novel MAO-B inhibitors, the chalcone 1, 3-diphenyl-2- propen-1-one (**1**, Fig. 1B) has emerged as a valid scaffold for the rational design of lead compounds. A number of naturally occurring or synthetic chalcones that bearing various groups on the A or B ring have demonstrated noticeable inhibitory effects on MAO-B[16–18]. The heterocyclic chalcones have been investigated as well[19]. Mathew et al.[20] had synthesised a series of chlorinated thienyl chalcone derivatives and found the most potent compound **TC6** exhibit an inhibitory activity with a $K_i$ values of 0.31 μM.

Interestingly, chalcone compounds have also been found to demonstrate anti-inflammatory activities in LPS stimulated cells[21]. Inspired by these results, we hypothesize that a novel series of chalcone compounds combing potent MAO-B-inhibiting and anti-neuroinflammation activities are feasible, which would exhibit improved therapeutic benefits for the management of PD and AD.

We previously investigated and reported the 1, 4-benzodioxan-substituted chalcone (*E*)−3-(2,3-dihydrobenzo[*b*][1,4]dioxin-6-yl)−1- phenylprop-2-en-1-one (**4a**) and its derivatives as potent selective and reversible MAO-B inhibitors[22]. Guided by the facts in the structure-activity relationship (SAR) study, we focused on the structural optimization of **4a** by replacing its A ring with heterocyclic rings including furan, thiophene and pyrrole. This work reports the design, synthesis, and evaluation of a series of 1, 4-benzodioxan-substituted thienyl chalcone derivatives as novel MAO-B inhibitors (Fig. 1B). The SAR is discussed and summarized. The hit compound is further evaluated for anti-inflammatory activities in activated microglia. In addition, the neuroprotective activity of the active compound against beta-Amyloid1-42($A\beta_{1-42}$)-induced cytotoxicity has also been assessed in microglia.

## Materials and methods

### General methods

The 2-acetyl heteroaromatics and aromatic aldehydes were purchased from Energy Chemical Company (Shanghai, China). Other reagents and solvents were commercially available and were used without further purification. Reactions were monitored by TLC on a glass plate coated with silica gel with fluorescent indicator (GF254). Column chromatography was performed on silica gel (200 – 300 mesh). $^1$H NMR and $^{13}$C NMR spectra were recorded using TMS as an internal standard with a Bruker BioSpin Ultrashield 400 NMR system. The purities of compounds used for biological evaluation (> 95%) were determined on a Waters Ultimate HPLC system using UV monitor at 254 and 365 nm for detection. The compounds were eluted with Acetonitrile/water (0.1% TFA, w/v) in ratios of 20:80–75:25 at a flow rate of 0.3 mL/min. The Compounds purities were calculated as the percentage peak area of the analysed compound, and retention times ($t_R$) were presented in minutes. High

resolution mass spectra (HRMS) were recorded on Agilent Technologies 6530 Q-TOF. The human recombinant MAO-A and -B enzymes, Amplex Red reagent, horseradish peroxidase, rasagiline and safinamide were obtained from Sigma Aldrich.

## Synthesis of chalcone compounds

### General procedure for the synthesis of heterocyclic chalcone derivatives 2–22

The heterocyclic chalcone derivatives **2**–**22** were synthesized according to the synthetic protocol outlined in Fig. 2. The 2-acetyl heteroaromatics (1 mmol) and corresponding aromatic aldehyde (1 mmol) were dissolved in 2 mL methanol. Then 2 ml 50% NaOH was added. The mixture was kept stirred at room temperature and the reaction was monitored by TLC until completed. Under ice bath, the mixture was diluted with water and adjusted to pH = 2–3 with 5% HCl. The precipitate formed was filtered off and then purified by chromatography column with ethyl acetate/petroleum ether or recrystallization with ethanol.

The purities of all the synthetic compounds determined by ultimate HPLC were greater than 95%. The structures of these compounds were confirmed by NMR spectroscopy and HRMS. Moreover, the structure of **12** was established by X-ray diffraction analysis (Fig. 3).

**(*E*)−3-phenyl-1-(thiophen-2-yl)prop-2-en-1-one (2)** Yield 42.4%; UPLC purity 99.90%, $t_R$=1.413 min。 $^1$H NMR (400 MHz, DMSO-$d_6$) $\delta$ 8.37 (s, 1H), 8.08 (s, 1H), 7.94–7.89 (m, 3 H), 7.77 (d, $J$ = 15.5 Hz, 1H), 7.48

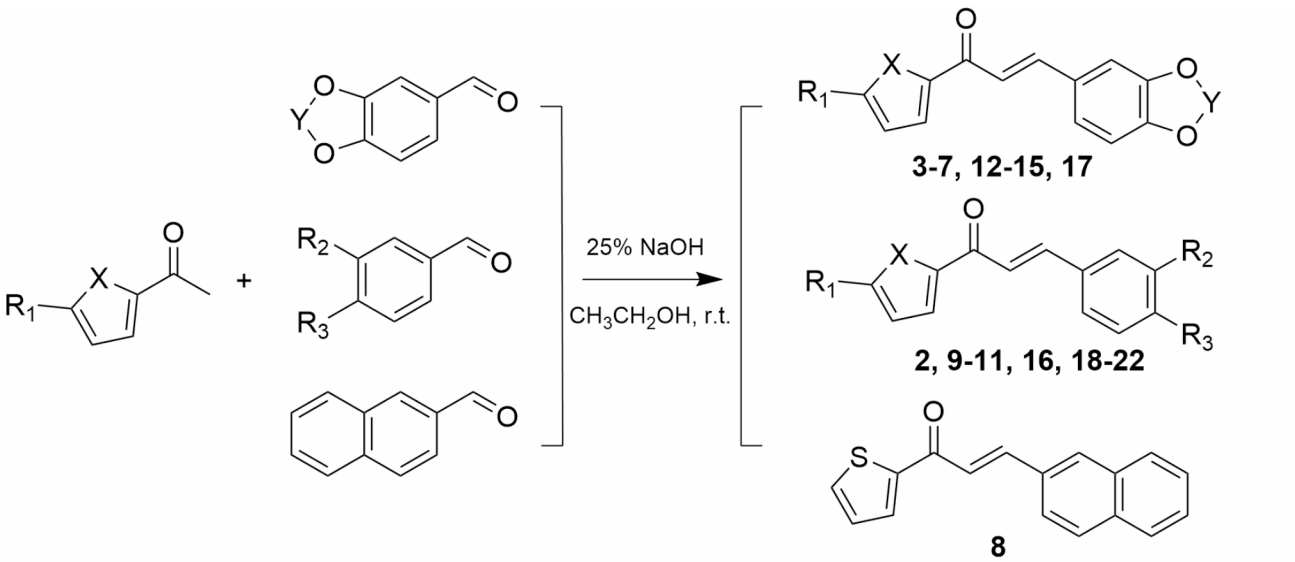


| Cpd | X | Y | $R_1$ | $R_2$ | $R_3$ |
|---|---|---|---|---|---|
| **2** | S | - | H | H | H |
| **3** | S | $C_2H_4$ | H | - | - |
| **4** | O | $C_2H_4$ | H | - | - |
| **5** | O | $C_2H_4$ | $CH_3$ | - | - |
| **6** | NH | $C_2H_4$ | H | - | - |
| **7** | S | $CH_2$ | H | - | - |
| **9** | S | - | H | H | $OCH_3$ |
| **10** | S | - | H | $OCH_3$ | $OCH_3$ |
| **11** | S | - | H | OH | $OCH_3$ |
| **12** | S | $C_2H_4$ | Cl | - | - |

| Cpd | X | Y | $R_1$ | $R_2$ | $R_3$ |
|---|---|---|---|---|---|
| **13** | S | $C_2H_4$ | Br | - | - |
| **14** | S | $C_2H_4$ | $CH_3$ | - | - |
| **15** | S | $CH_2$ | Cl | - | - |
| **16** | S | - | Cl | $OCH_3$ | $OCH_3$ |
| **17** | S | $CH_2$ | Br | - | - |
| **18** | S | - | Br | $OCH_3$ | $OCH_3$ |
| **19** | S | - | $CH_3$ | OH | $OCH_3$ |
| **20** | O | - | H | OH | $OCH_3$ |
| **21** | O | - | $CH_3$ | OH | $OCH_3$ |
| **22** | NH | - | H | OH | $OCH_3$ |

**Fig. 2**. Synthesis of chalcone derivatives **2**–**22**.

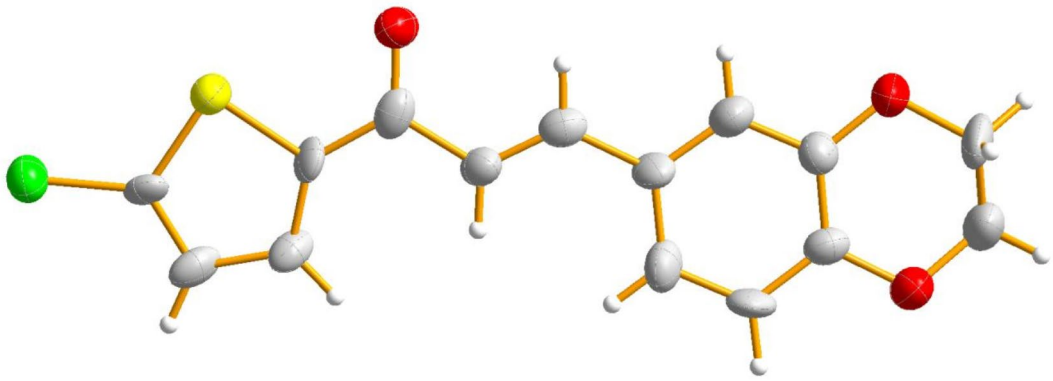

**Fig. 3**. Diagram of compound **12** (ellipsoid 50%).

(s,3 H), 7.34(d, $J$ = 4.5 Hz, 1H). $^{13}$C NMR (101 MHz, DMSO-$d_6$) $\delta$ 182.08, 145.95, 143.63,136.06, 134.96, 134.20, 131.13, 129.38, 122.36. m/z $[M+H]^+$ calcd for $C_{13}H_{10}OS$: 215.0531, found: 215.0520.

**(*E*)−3-(2, 3-dihydrobenzo[*b*][1,4]dioxin-6-yl)−1-(thiophen-2-yl)prop-2-en-1-one (3)** Yield 40.0%; UPLC purity 98.99%, $t_R$=6.647 min。$^1$H NMR (400 MHz, DMSO-$d_6$) $\delta$ 8.34(d, $J$ = 3.7 Hz, 1H), 8.04 (d, $J$ = 4.8 Hz, 1H), 7.76 (d, $J$ = 15.5 Hz, 1H), 7.64 (d, $J$ = 15.5 Hz, 1H), 7.52 (d, $J$ = 2.1 Hz, 1H), 7.38 (dd, $J$ = 8.4, 2.1 Hz, 1H), 7.32 (t, $J$ = 4.3 Hz, 1H), 6.94 (d, $J$ = 8.3 Hz, 1H), 4.31(q, $J$ = 5.0, 4.4 Hz, 4 H). $^{13}$C NMR (101 MHz, DMSO-$d_6$) $\delta$ 181.99, 146.37, 146.25, 144.08, 143.49, 135.69, 133.86, 129.31, 128.47, 123.59, 120.42, 117.90, 117.67, 64.88, 64.42. m/z $[M+H]^+$ calcd for $C_{15}H_{12}O_3S$: 273.0580, found: 273.0663.

**(*E*)−3-(2, 3-dihydrobenzo[*b*][1,4]dioxin-6-yl)−1-(furan-2-yl)prop-2-en-1-one (4)** Yield 42.3%; UPLC purity 99.88%, $t_R$=1.262 min。$^1$H NMR (400 MHz, DMSO-$d_6$) $\delta$ 8.06 (d, $J$ = 1.6 Hz, 1H), 7.83 (d, $J$ = 3.6 Hz, 1H), 7.65 (d, $J$ = 15.6 Hz, 1H), 7.57 (d, $J$ = 15.6 Hz,1H), 7.47 (d, $J$ = 2.1 Hz, 1H), 7.35 (dd, $J$ = 8.3, 2.1 Hz, 1H), 6.94 (d, $J$ = 8.4 Hz, 1H), 6.79 (dd, $J$ = 3.6, 1.7 Hz, 1H),4.30 (q, $J$ = 5.1 Hz, 4 H). $^{13}$C NMR (101 MHz, DMSO-*d6*) $\delta$ 177.05, 153.51, 148.64, 146.33, 144.07, 143.09, 128.39, 123.38, 120.50, 119.69, 117.92, 117.60, 113.10, 64.87, 64.41. m/z $[M+H]^+$ calcd for $C_{15}H_{12}O_4$: 257.0814, found: 257.0842.

**(*E*)−3-(2, 3-dihydrobenzo[*b*][1,4]dioxin-6-yl)−1-(5-methylfuran-2-yl)prop-2-en-1-one (5)** Yield 63.3%; UPLC purity 99.96%, $t_R$=1.356 min。$^1$H NMR (400 MHz, DMSO-$d_6$) $\delta$ 7.75 (d $J$ = 3.5 Hz, 1H), 7.59 (d, $J$ = 15.6 Hz, 1H), 7.50 (d, $J$ = 15.6 Hz, 1H), 7.44 (d, $J$ = 2.0 Hz,1H), 7.32 (dd, $J$ = 8.4, 2.1 Hz, 1H), 6.92 (d, $J$ = 8.3 Hz, 1H), 6.43 (d, $J$ = 3.4 Hz, 1H), 4.29 (q, $J$ = 5.1 Hz, 4 H), 2.40(s, 3 H). $^{13}$C NMR (101 MHz, DMSO-$d_6$) $\delta$ 176.23, 158.75, 152.45, 146.18,144.07, 142.41, 128.50, 123.23, 121.52, 120.61, 117.90, 117.50, 109.83, 64.86, 64.43, 14.19. m/z $[M+H]^+$ calcd for $C_{16}H_{14}O_4$: 271.0970, found: 271.0956.

**(*E*)−3-(2, 3-dihydrobenzo[*b*][1,4]dioxin-6-yl)−1-(1*H*-pyrrol-2-yl)prop-2-en-1-one (6)** Yield 61.3%; UPLC purity 99.78%, $t_R$=1.224 min。$^1$H NMR (400 MHz, DMSO-$d_6$) $\delta$ 11.94 (s, 1H), 7.54 (s, 2 H), 7.43 (d, $J$ = 2.0 Hz, 1H), 7.35–7.30(m, 2 H), 7.14 (d, $J$ = 2.9 Hz,1H), 6.91 (d, $J$ = 8.3 Hz, 1H), 6.27–6.25 (m, 1H), 4.29 (q, $J$ = 4.6 Hz, 4 H). $^{13}$C NMR (101 MHz, DMSO-$d_6$) $\delta$ 178.33, 145.82, 144.06, 140.95, 133.61, 128.89, 126.51, 122.94, 121.71, 117.84, 117.52, 117.30, 110.52, 64.84, 64.44.m/z $[M-H]^-$ calcd for $C_{15}H_{12}NO_3$: 254.0864, found: 254.0818.

**(*E*)−3-(benzo[*d*][1,3]dioxol-5-yl)−1-(thiophen-2-yl)prop-2-en-1-one (7)** Yield 90.8%; UPLC purity 99.69%, $t_R$=1.379 min。$^1$H NMR (400 MHz, DMSO-$d_6$) $\delta$ 8.34 (d, $J$ = 3.8 Hz, 1H), 8.05 (d, $J$ = 4.9 Hz, 1H), 7.78 (d, $J$ = 15.5 Hz, 1H), 7.70–7.66 (m, 2 H), 7.36–7.32 (m, 2 H), 7.01 (d, $J$ = 8.0 Hz,1H), 6.13 (s, 2 H). $^{13}$C NMR (101 MHz, DMSO-$d_6$) $\delta$ 181.99, 150.09, 148.57, 146.27, 143.61, 135.70, 133.84, 129.49, 129.29, 126.47, 120.31, 109.00, 107.40,102.15. m/z $[M+H]^+$ calcd for $C_{14}H_{10}O_3S$: 259.0429, found: 259.0418.

**(*E*)−3-(naphthalen-2-yl)−1-(thiophen-2-yl)prop-2-en-1-one (8)** Yield 85.4%; UPLC purity 99.76%, $t_R$=1.535 min。$^1$H NMR (400 MHz, DMSO-$d_6$) $\delta$ 8.43 (s, 1H), 8.36 (s, 1H), 8.17–7.91 (m, 7 H), 7.63–7.57 (m, 2 H), 7.37 (s, 1H). $^{13}$C NMR (101 MHz, DMSO-$d_6$) $\delta$ 182.05, 146.06, 143.64, 136.09, 134.41, 134.22, 133.41, 132.65, 131.30, 129.41, 129.00, 128.94, 128.20,127.95, 127.29, 124.83, 122.67. m/z $[M+H]^+$ calcd for $C_{17}H_{12}OS$: 265.0687, found: 265.0677.

**(*E*)−3-(4-methoxyphenyl)−1-(thiophen-2-yl)prop-2-en-1-one (9)** Yield 41.7%; UPLC purity 99.78%, $t_R$=1.393 min。$^1$H NMR (400 MHz, DMSO-$d_6$) $\delta$ 8.32 (d, $J$ = 3.2 Hz, 1H), 8.05 (d, $J$ = 4.6 Hz, 1H), 7.87 (d, $J$ = 8.2 Hz, 2 H), 7.79 −7.70 (m, 2 H),7.32 (t, $J$ = 4.1 Hz, 1H), 7.04 (d, $J$ = 8.1 Hz,2 H), 3.83 (s, 3 H). $^{13}$C NMR(101 MHz, DMSO-$d_6$) $\delta$ 182.00, 161.87, 146.26,143.58, 135.61, 133.69, 131.29, 129.29,127.60, 119.84, 114.88, 55.85. m/z $[M+H]^+$ calcd for $C_{14}H_{12}O_2S$: 245.0636, found: 245.0625.

**(*E*)−3-(3, 4-dimethoxyphenyl)−1-(thiophen-2-yl)prop-2-en-1-one (10)** Yield 83.6%; UPLC purity 99.68%, $t_R$=1.344 min。$^1$H NMR (400 MHz, DMSO-$d_6$) $\delta$ 8.35 (d, $J$ = 3.7 Hz, 1H), 8.05 (d, $J$ = 4.9 Hz, 1H), 7.78 (d, $J$ = 15.5 Hz, 1H), 7.71(d,$J$ = 15.4 Hz, 1H), 7.55 (s, 1H), 7.41 (dd, $J$ = 8.3, 2.0 Hz,1H), 7.33 (t, $J$ = 4.4 Hz, 1H), 7.04 (d, $J$ = 8.3 Hz, 1H), 3.88 (s, 3 H), 3.83 (s,3 H). $^{13}$C NMR (101 MHz, DMSO-$d_6$) $\delta$ 182.01, 151.80, 149.47, 146.30, 144.08,135.62, 133.76, 129.22, 127.77, 124.40, 119.89,112.02, 111.32, 56.20, 56.06. m/z$[M+H]^+$ calcd for $C_{15}H_{14}O_3S$: 275.0742, found: 275.0732.

**(*E*)−3-(3-hydroxy-4-methoxyphenyl)−1-(thiophen-2-yl)prop-2-en-1-one (11)** Yield 26.3%; UPLC purity 99.41%, $t_R$=1.287 min。$^1$H NMR (400 MHz, DMSO-$d_6$) $\delta$ 9.20 (s, 1H), 8.31 (d, $J$ = 3.7 Hz, 1H), 8.04 (d, $J$ = 4.9 Hz,

1H), 7.70–7.62 (m, 2 H), 7.37 (s, 1H), 7.33–7.30 (m, 2 H), 7.02 (d, *J* = 8.3 Hz, 1H), 3.86 (s, 3 H). m/z $[M+H]^+$ calcd for $C_{14}H_{12}O_3S$: 261.0585, found: 261.0576.

**(*E*)−1-(5-chlorothiophen-2-yl)−3-(2, 3-dihydrobenzo[*b*][1,4]dioxin-6-yl)prop-2-en-1-one** (**12**) Yield 58.2%; UPLC purity 98.99%, $t_R$=2.415 min。$^1$H NMR (400 MHz, DMSO-$d_6$) *δ* 8.25 (d, *J* = 4.1 Hz, 1H), 7.72 (d, *J* = 15.5 Hz, 1H), 7.63 (d, *J* = 15.5 Hz, 1H), 7.52(d, *J* = 2.0 Hz,1H), 7.38–7.36 (m, 2 H), 6.94 (d, *J* = 8.3 Hz, 1H), 4.30 (q, *J* = 5.2 Hz,4 H). $^{13}$C NMR (101 MHz, DMSO-$d_6$) *δ* 181.27, 146.58, 145.37, 144.12, 138.15, 133.93, 129.58, 128.35, 123.83, 119.25, 117.93, 117.75, 64.92, 64.43. m/z $[M+H]^+$ calcd for $C_{15}H_{11}ClO_3S$: 307.0196, found:307.0186.

**(*E*)−1-(5-bromothiophen-2-yl)−3-(2, 3-dihydrobenzo[*b*][1,4]dioxin-6-yl)prop-2-en-1-one** (**13**) Yield 28.0%;UPLC purity 95.29%, $t_R$=8.608 min。$^1$H NMR (400 MHz, DMSO-*d6*) *δ* 8.19 (d, *J* = 4.1 Hz, 1H), 7.72 (d, *J* = 15.5 Hz, 1H), 7.63 (d, *J* = 15.5 Hz, 1H), 7.52(d, *J* = 2.1 Hz,1H), 7.48 (d, *J* = 4.1 Hz, 1H), 7.37 (dd, *J* = 8.4, 2.1 Hz, 1H), 6.94 (d, *J* = 8.4 Hz, 1H), 4.30 (q, *J* = 5.2 Hz, 4 H). $^{13}$CNMR (101 MHz, DMSO-$d_6$) *δ* 181.06, 148.02, 146.55, 144.15, 144.09, 134.53,132.98, 128.35, 123.81, 122.48, 119.37, 117.91, 117.74,64.90, 64.41. m/z $[M+H]^+$ calcd for $C_{15}H_{11}BrO_3S$: 352.9670, found: 352.9661.

**(E)−3-(2, 3-dihydrobenzo[*b*][1,4]dioxin-6-yl)−1-(5-methylthiophen-2-yl)prop-2-en-1-one** (**14**) Yield 50.1%; UPLC purity 97.74%, $t_R$=1.992 min。$^1$H NMR (400 MHz, DMSO-$d_6$) *δ* 8.15 (d, *J* = 3.8 Hz, 1H), 7.69 (d, *J* = 15.5 Hz, 1H), 7.58 (d, *J* = 15.5 Hz, 1H), 7.49 (d, *J* = 2.1 Hz,1H), 7.35 (dd, *J* = 8.4, 2.1 Hz, 1H), 7.02(d, *J* = 3.0 Hz, 1H), 6.93 (d, *J* = 8.4 Hz, 1H), 4.30 (q, *J* = 5.5, 5.1 Hz, 4 H),2.54 (s, 3 H). $^{13}$C NMR (101 MHz, DMSO-$d_6$) *δ* 181.46, 150.44, 146.24, 144.14, 144.07, 142.89, 134.45, 128.53, 128.07, 123.46, 120.25, 117.88, 117.58, 64.87, 64.42, 16.22. m/z $[M+H]^+$ calcd for $C_{16}H_{14}O_3S$: 287.0742, found: 287.0728.

**(*E*)−3-(benzo[d][1,3]dioxol-5-yl)−1-(5-chlorothiophen-2-yl)prop-2-en-1-one** (**15**) Yield 90.8%; UPLC purity 99.99%, $t_R$=1.379 min。$^1$H NMR (400 MHz, DMSO-$d_6$) *δ* 8.25 (d, *J* = 4.1 Hz, 1H), 7.74 (d, *J* = 15.5 Hz, 1H), 7.68–7.65(m, 2 H), 7.38 (d, *J* = 4.1 Hz, 1H), 7.34 (d, *J* = 8.0 Hz, 1H), 7.01 (d, *J* = 8.0 Hz, 1H), 6.12 (s, 2 H). $^{13}$C NMR (101 MHz, DMSO-$d_6$) *δ* 181.23, 150.28, 148.59, 145.37, 144.21, 138.17, 133.89, 129.57, 129.37, 126.78, 119.09, 109.03, 107.40, 102.21. m/z $[M+H]^+$ calcd for $C_{14}H_9ClO_3S$: 293.0034, found: 293.0031.

**(*E*)−1-(5-chlorothiophen-2-yl)−3-(3, 4-dimethoxyphenyl)prop-2-en-1-one** (**16**) Yield 59.0%; UPLC purity 99.64%, $t_R$=1.478 min。$^1$H NMR (400 MHz, DMSO-$d_6$) *δ* 8.26 (d, *J* = 4.1 Hz, 1H), 7.76–7.67 (m, 2 H), 7.53 (s, 1H), 7.42 −7.39 (m, 2 H), 7.04 (d, *J* = 8.3 Hz, 1H), 3.87 (s, 3 H), 3.83 (s, 3 H). $^{13}$C NMR (101 MHz, DMSO-$d_6$) *δ* 181.23, 151.98, 149.47, 145.40, 144.67, 138.08, 133.79, 129.47, 127.63, 124.67, 118.65, 112.01, 111.35, 56.20, 56.08. m/z $[M+H]^+$ calcd for $C_{15}H_{13}ClO_3S$: 309.0352, found: 309.0343.

**(*E*)−3-(benzo[*d*][1,3]dioxol-5-yl)−1-(5-bromothiophen-2-yl)prop-2-en-1-one** (**17**) Yield 40.2%; UPLC purity 99.26%, $t_R$=1.526 min。$^1$H NMR (400 MHz, DMSO-$d_6$) *δ* 8.18 (d, *J* = 4.1 Hz, 1H), 7.74–7.65 (m, 3 H), 7.48 (d, *J* = 3.9 Hz, 1H), 7.34 (d, *J* = 8.1 Hz, 1H), 7.00 (d, *J* = 8.5 Hz, 1H), 6.12 (s, 2 H). $^{13}$CNMR (101 MHz, DMSO-$d_6$) *δ* 181.04, 150.26, 148.58, 148.03, 144.24, 134.48, 132.96, 129.39, 126.74, 122.49, 119.26, 109.01, 107.40, 102.20. m/z $[M+H]^+$ calcd for $C_{14}H_9BrO_3S$: 338.9514, found: 338.9505.

**(*E*)−1-(5-bromothiophen-2-yl)−3-(3, 4-dimethoxyphenyl)prop-2-en-1-one** (**18**) Yield 25.2%; UPLC purity 96.80%, $t_R$=1.435 min。$^1$H NMR (400 MHz, DMSO-$d_6$) *δ* 8.19 (d, *J* = 4.1 Hz, 1H), 7.71 (s, 2 H), 7.53 (d, *J* = 2.0 Hz, 1H), 7.49 (d, *J* = 4.0 Hz,1H), 7.41 (dd, *J* = 8.3, 2.0 Hz, 1H), 7.03 (d, *J* = 8.3 Hz,1H), 3.87 (s, 3 H), 3.83 (s, 3 H).$^{13}$C NMR (101 MHz, DMSO-$d_6$) *δ* 181.05, 151.97, 149.47, 148.05, 144.72, 134.39, 132.88, 127.66, 124.66, 122.39, 118.81, 112.00, 111.31, 56.19, 56.07. m/z $[M+Na]^+$ calcd for $C_{15}H_{13}BrO_3S$: 374.966, found:374.971.

**(*E*)−3-(3-hydroxy-4-methoxyphenyl)−1-(5-methylthiophen-2-yl)prop-2-en-1-one** (**19**) Yield 36.7%;UPLC purity 96.47%, $t_R$=6.593 min。$^1$H NMR (400 MHz, DMSO-$d_6$) *δ* 9.17 (s,1H), 8.12 (d, *J* = 3.8 Hz, 1H), 7.63–7.55 (m, 2 H), 7.33–7.27 (m, 2 H), 7.00(d, *J* = 8.1 Hz, 2 H), 3.85 (s, 3 H), 2.54 (s, 3 H). $^{13}$C NMR (101 MHz, DMSO-$d_6$) *δ* 181.45, 150.69, 150.24, 147.09, 144.14, 143.51, 134.19, 128.06, 127.98, 122.48, 119.54, 115.32, 112.33, 56.14, 16.20. m/z $[M+H]^+$ calcd for $C_{15}H_{14}O_3S$: 275.0736, found: 275.0737.

**(*E*)−1-(furan-2-yl)−3-(3-hydroxy-4-methoxyphenyl)prop-2-en-1-one** (**20**) Yield 15.9%; UPLC purity 96.8%, $t_R$=5.331 min。$^1$H NMR (400 MHz, DMSO-$d_6$) *δ* 9.21 (s, 1H), 8.06 (s, 1H), 7.78 (d, *J* = 3.6 Hz, 1H), 7.64 (d, *J* = 15.5 Hz, 1H), 7.48 (d, *J* = 15.6 Hz, 1H), 7.31 (d, *J* = 2.1 Hz, 1H), 7.27 (dd, *J* = 8.3, 2.1 Hz, 1H), 7.01 (d, *J* = 8.3 Hz, 1H), 6.79–6.78 (m, 1H), 3.85 (s, 3 H).$^{13}$C NMR (101 MHz, DMSO-$d_6$) *δ* 177.14, 153.56, 150.81, 148.48, 147.14, 143.73, 127.83, 122.57, 119.70, 119.32, 115.13, 113.13, 112.36, 56.14. m/z $[M+H]^+$ calcd for $C_{14}H_{12}O_4$: 245.0808, found: 245.0804.

**(*E*)−3-(3-hydroxy-4-methoxyphenyl)−1-(5-methylfuran-2-yl)prop-2-en-1-one** (**21**) Yield 61.5%; UPLC purity 95.55%, $t_R$=5.710 min。$^1$H NMR (400 MHz, DMSO-$d_6$) *δ* 9.21 (s,1H), 7.70 (d, *J* = 3.5 Hz, 1H), 7.58 (d, *J* = 15.6 Hz, 1H), 7.42 (d, *J* = 15.6 Hz, 1H), 7.29 (s, 1H), 7.24 (dd, *J* = 8.4, 2.2 Hz, 1H), 6.99(d, *J* = 8.3 Hz, 1H), 6.42 (d, *J* = 3.4 Hz, 1H), 3.83 (s, 3 H), 2.41 (s, 3 H). $^{13}$CNMR (101 MHz, DMSO-$d_6$) *δ* 176.35, 158.56, 152.49, 150.67,147.13, 143.07, 127.93, 122.40, 121.13, 119.78, 115.04, 112.37, 109.86, 56.14, 14.19. m/z $[M+H]^+$ calcd for $C_{15}H_{14}O_4$: 259.0965, found: 259.0962.

**(*E*)−3-(3-hydroxy-4-methoxyphenyl)−1-(1*H*-pyrrol-2-yl)prop-2-en-1-one** (**22**) Yield 38.3%; UPLC purity 95.38%, $t_R$=5.702 min。$^1$H NMR (400 MHz, DMSO-$d_6$) *δ* 11.95(s, 1H), 9.15 (s, 1H), 7.56 (d, *J* = 15.6 Hz, 1H), 7.47 (d, *J* = 15.6 Hz, 1H), 7.32– 7.29 (m, 2 H), 7.25 (dd, *J* = 8.3, 2.1 Hz, 1H), 7.15 (s, 1H), 6.99 (d, *J* = 8.3 Hz, 1H),6.27 (dt, *J* = 4.3, 2.3 Hz, 1H), 3.84 (s, 3 H). $^{13}$CNMR (101 MHz, DMSO-$d_6$) *δ* 178.36, 150.26, 147.08, 141.57, 133.60, 128.30, 126.40, 121.94, 120.91, 117.23, 115.05, 112.36, 110.53, 56.12. m/z $[M+H]^+$calcd for $C_{14}H_{13}NO_3$: 244.0968, found: 244.0982.

## X-ray data collection & structure refinement of compound 12

The structure of the **12** was solved using single X-ray diffractometry (Fig. 3). Crystal Data for compound **12** [$C_{15}H_{11}ClO_3S$ (*M* = 306.75 g/mol)]: monoclinic, space group $P2_1/c$ (no. 14), a = 14.0110(10) Å, b = 17.3889(12) Å, c = 11.0981(6) Å, β = 96.703(3), V = 2685.4(3) Å$^3$, Z = 8, T = 150.0 K, μ(GaKα) = 2.616 mm$^{-1}$, $D_{calc}$ = 1.517 g/cm$^3$, 50,329 reflections measured (5.526° ≤ 2θ ≤ 119.022°), 5890 unique ($R_{int}$ = 0.0633, $R_{sigma}$ = 0.0407) which

were used in all calculations. The final $R_1$ was 0.0453 ($I > 2\sigma(I)$) and $wR_2$ was 0.1197 (all data). The experimental details are depicted in Supplementary materials.

## *h*MAO Inhibition assay

The hMAO inhibition assay was performed as previously described[23]. Adequate amounts of recombinant *h*MAO-A/B were acquired and adjusted to 12.5 μg/mL or 75 μg/mL for *h*MAO-A or *h*MAO-B, respectively, with sodium phosphate buffer (50 mM, pH 7.4). The test compounds were dissolved in DMSO as stock solutions (10 mM) and diluted with sodium phosphate buffer (50 mM, pH 7.4) to the corresponding concentrations. Then the test compounds (20 μL) and *h*MAO (80 μL) were incubated for 15 min at 37 °C in a flat, black-bottomed 96-well microtest plate in the dark. The reaction was initiated by adding Amplex Red reagent (200 μM, final concentration), horseradish peroxidase (2 U/mL, final concentration), and 2 mM p-tyramine for *h*MAO-A or 2 mM benzylamine (final concetration) for hMAO-B and incubated at 37 °C for 20 min. Activity was quantified in a multi detection microplate fluorescence reader (SpectraMax M5, Molecular Devices, USA) based on the fluorescence generated (excitation, 545 nm; emission, 590 nm).The specific fluorescence emission was calculated after subtraction of the background activity. The background activity was determined from wells containing all components except the *h*MAO isoforms, which were replaced by a sodium phosphate buffer solution. The percentage inhibition was calculated by the following expression: $(1 - I_{Fi} / I_{Fc}) \times 100$, in which $I_{Fi}$ and $I_{Fc}$ are the fluorescence intensities obtained for *h*MAO in the presence and absence of inhibitors after subtracting the respective background. The synthetic compounds were first screened for the inhibition of *h*MAO-B at 1 μM, which showed more than 60% enzyme inhibition were then subjected to $IC_{50}$ determination.

## Enzyme kinetic study

To evaluate the mode of MAO-B inhibition, the representative compound was evaluated in substrate-dependent kinetic experiments performed as previously described[22]. Sets of Lineweaver–Burk plots were generated. The reciprocal MAO-B activity was plotted against the reciprocal substrate concentration. The initial catalytic rates of *h*MAO-B were measured at four different concentrations of the substrate benzylamine (0.5, 1, 1.5 and 2 mM) in the absence (basal sample) and in the presence of five different concentrations (0, $IC_{50}$, 3/2 $IC_{50}$ 2 $IC_{50}$ and 5/2 $IC_{50}$) of the inhibitors. The enzymatic reactions and measurements were performed using *h*MAO-B assay conditions as described above for the determination of $IC_{50}$ values.

## Dialysis assay

To further confirm the inhibitory reversibility of the MAO-B inhibition by the active compound, The dialysis assay was performed according to previously described method[24,25]. Dialysis membrane with a molecular weight cutoff of 14 kDa was bought from Viskase. The MAO enzymes (0.03 mg protein/mL) were combined with the test inhibitors at a concentration equal to $4\times IC_{50}$ for the inhibition of the MAO-B. The irreversible inhibitor *R*-(-)-deprenyl [$IC_{50} = 0.079$ μM] was employed as the reference compound. The volume of these mixtures was 0.5 mL and potassium phosphate buffer (100 mM, pH 7.4, 5% sucrose) containing 4% DMSO served as solvent. The mixtures were individually dialyzed at 4 ℃ in 50 mL of dialysis buffer (100 mM potassium phosphate, pH 7.4, 5% sucrose). The dialysis buffer was replaced with fresh buffer at 3 h and 7 h after the start of dialysis. After 24 h, the mixture of enzyme and inhibitors was warmed to 37 ℃ and the enzyme activity was determined as described above. For comparison, undialyzed mixtures of the MAO-B and the inhibitors were included in the study.

## Molecular Docking study

A molecular docking study was performed to investigate the possible interaction between the active compounds and *h*MAOs. The crystal structures of *h*MAO-B (PDB code 2V61)[26] and *h*MAO-A (PDB code 2z5x)[27] were adopted and the compounds were docked into the active sites following the standard dock protocol in the software Molecular Operating Environment (MOE) 2022. For the docking into *h*MAO-B, nine conserved water molecules were included in the docking process according to previous reports[28]. Default settings were used, unless stated otherwise. The poses of the docked compounds are ranked by the scores from the GBVI/WSA binding free energy calculation and the top-ranked one was selected and analysed.

## Studies of inhibiting NO, TNF-α and IL-1β production in activated BV2 microglial cells

The studies of inhibiting NO, TNF-αand IL-1β production in activated BV2 microglial cells were performed according to the previous report[29].BV2 Cells were plated at $4\times10^4$ cells per well and allowed to grow at 37 °C for 48 h. Then the cells were pre-treated with various concentrations of the tested compounds for 6 h at 37 °C in a humidified atmosphere with 5% $CO_2$, 0.5% DMSO acted as the vehicle control. The cell culture medium was then removed, followed by the addition of 100 μL DMEM, LPS (100 ng/mL, final concentration) and $A\beta_{1-42}$ (15 μM, final concentration), respectively. The cells were incubated at 37 °C for 24 h. The level of NO in the culture medium was measured by using a nitric oxide assay kit (Beyotime Biotechnology) in accordance with the manufacturer's instructions. The levels of TNF-α and IL-1β in the culture medium were measured by using ELISA kits (Beyotime Biotechnology) in accordance with the manufacturer's instructions.

## MTT assay

The 3-(4, 5-dimethylthiazol-2-yl)−2,5-diphenyltetrazolium (MTT) assay was performed as previously described[22]. BV2 or SHSY5Y Cells were plated at 5000 cells per well and allowed to grow at 37 °C overnight. (1) To evaluate the cytotoxicity of compounds, the BV2 or SHSY5Y cells were treated with various concentrations of the tested compounds for 24 h; (2) To evaluate the cytotoxicity induced by $A\beta_{1-42}$, BV2 cells were treated with various concentrations of $A\beta_{1-42}$ for 24 h; (3) To evaluate the neuroprotective effect of the compounds, BV2 cells were pre-treated with various concentrations of the tested compounds for 24 h, then $A\beta_{1-42}$ (15 μM, final

concentration) was added and incubated for 24 h. In the above assays, 0.5% DMSO acted as the vehicle control. After the treatment, The cell culture medium was then removed, followed by the addition of fresh cell culture medium containing 5.0 g/L MTT (20 µL / per well) and incubation at 37 °C in a humidified, 5% $CO_2$ atmosphere for 4 h. After this incubation period, the cell culture medium was removed and the formed formazan crystals dissolved in 100% DMSO. The absorbance was measured at 570 nm in a multi-well plate reader. The results are expressed as % relative cell viability compared to DMSO vehicle control.

## Results

### Inhibitory activities of monoamine oxidase

All the synthetic chalcone derivatives were sceened for the inhibitory effects on human MAO-B and MAO-A using a fluorescence-based assay. The tested concentration was 1 µM unless otherwise stated. The irreversible inhibitor rasagiline and reversible inhibitor safinamide were used as positive controls for *h*MAO-B inhibition. Clorgyline was used as a positive control for *h*MAO-A inhibition.

As shown in Table 1, both rasagiline and safinamide exhibited significant inhibitory activities on *h*MAO-B, which exhibited 90.1% and 86.9% inhibition on *h*MAO-B at 1 µM with $IC_{50}$values of 0.096 µM and 0.060 µM respectively, which are comparable to that of previous reports[26,30]. The parent chalcone compound **1** exhibited a moderate inhibition effect against *h*MAO-B (41.6% inhibition at 10 µM) with an $IC_{50}$ of 13.04 µM. Replacing the phenyl ring of **1** with the thienyl moiety (**2**) resulted in increased inhibitory activity (23.79% inhibition at 1µM, $IC_{50}$= 10.62 µM), which suggested that the thienyl substitution may be favourable. Inspired by the fact that the 1, 4-benzodioxan moiety is privileged scaffold for the design of MAO-B inhibitors[22], we tried to replace the phenyl ring of **2** with the 1, 4-benzodioxan moiety and found that the resulted compound ( **3**) exhibited a 17-fold higher *h*MAO-B inhibition (72.8% inhibition at 1 µM, $IC_{50}$ = 0.61 µM) than **2**. As replacing the thienyl moiety of **3** with the furan (**4**–**5**) or pyrrole (**6**) moieties resulted in much lower inhibitory activities (32.5%、47.8% and 42.2% inhibition, respectively), we hypothesized that compound **3**, a new 1, 4-benzodioxan-substituted thienyl chalcone derivative, could serve as a potential scaffold for the design of novel *h*MAO-B inhibitors.

As for compound **3**, replacing the 1, 4-benzodioxan moiety with the 1, 3-dioxaindane or naphthyl decreased the inhibitory activity. The corresponding compounds **7**, **8** showed only 56.3% and 27% inhibition respectively. Cleaving the 1, 4-dioxan ring of **3** led to the $-OCH_3$ substituted compounds **9**–**11**, which also exhibited much lower inhibitory activities (51.7%、<5% and 16.6% inhibition, respectively) compared to compound **3**. These results clearly indicate that the 1, 4-benzodioxan moiety is crucial for the inhibitory activity of compound **3**.

| | hMAO-A | hMAO-B | | |
|---|---|---|---|---|
| Compound | $IC_{50}$ (µM) | Inhibition (%) | $IC_{50}$ (µM) | Selectivity Index (SI)[a] |
| 1 | > 40 | 41.6% ± 0.003[b] | 13.04 ± 0.06 | > 3 |
| 2 | > 40 | 23.8% ± 0.1 | 10.62 ± 1.4 | > 3 |
| 3 | > 40 | 72.8% ± 5.8 | 0.61 ± 0.12 | > 65 |
| 4 | > 40 | 32.5% ± 9.6 | N.D. | - |
| 5 | > 40 | 47.8% ± 1.6 | N.D. | - |
| 6 | > 40 | 42.2% ± 1.4 | N.D. | - |
| 7 | > 40 | 56.3% ± 0.6 | N.D. | N.D. |
| 8 | > 40 | 27% ± 3.2 | N.D. | N.D. |
| 9 | > 40 | 51.7% ± 0.8 | N.D. | N.D. |
| 10 | > 40 | < 5% | N.D. | N.D. |
| 11 | > 40 | 16.6% ± 1.2 | N.D. | N.D. |
| 12 | > 40 | 89.5% ± 0.7 | 0.11 ± 0.02 | > 363 |
| 13 | > 40 | 83.8% ± 1.8 | 0.12 ± 0.02 | > 333 |
| 14 | > 40 | 69.9% ± 3.0 | 0.27 ± 0.05 | > 148 |
| 15 | > 40 | 73.5% ± 4.2 | 0.43 ± 0.07 | > 93 |
| 16 | > 40 | 14.5% ± 0.03 | N.D. | N.D. |
| 17 | > 40 | 77.5% ± 2.0 | 0.80 ± 0.06 | > 50 |
| 18 | > 40 | 12.3% ± 2.1 | N.D. | N.D. |
| 19 | > 40 | 28.2% ± 6.8 | N.D. | N.D. |
| 20 | > 40 | < 5% | N.D. | N.D. |
| 21 | > 40 | < 5% | N.D. | N.D. |
| 22 | > 40 | < 5% | N.D. | N.D. |
| Rasagiline | N.D. | 90.1% ± 0.9 | 0.096 ± 0.01 | N.D. |
| Safinamide | N.D. | 86.9% ± 0.7 | 0.060 ± 0.001 | N.D. |
| Clorgyline | 79.9% ± 0.46 [c] | N.D. | N.D. | N.D. |

**Table 1**. *h*MAO inhibitory activities of 1, 4-benzodioxan-substituted Thienyl chalcone derivatives. The data are represented as means ± SD from at least three independent experiments. [a]Selectivity index (SI) = $IC_{50}$ (hMAO-A) / $IC_{50}$ (hMAO-B); [b]inhibition at 10 µM. 6; [c]% inhibition at 0.1 µM; N.D., no determined;.

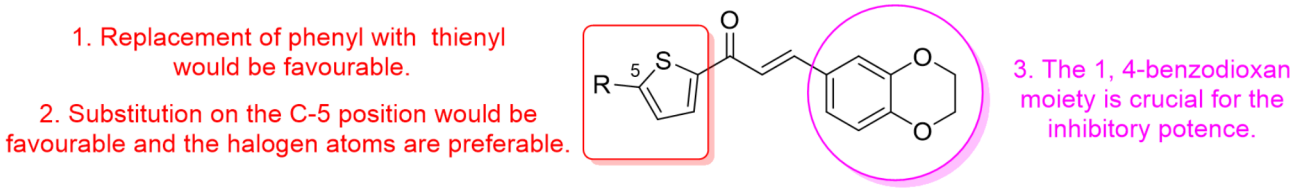


**Fig. 4**. The SAR of 1, 4-benzodioxan -substituted thienyl chalcone compounds towards *h*MAO-B inhibition.

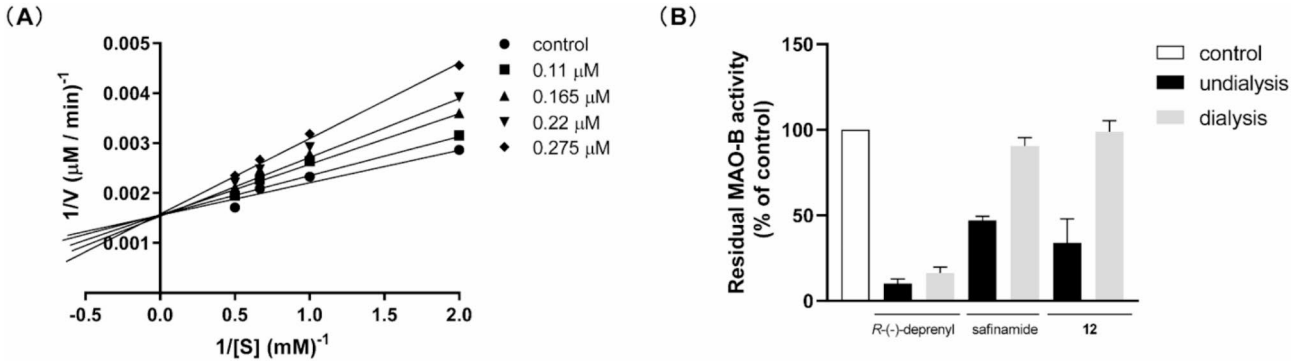


**Fig. 5**. (**A**) The Lineweaver–Burk plot for *h*MAO-B inhibition by compound **12**;. (**B**) The dialysis study of MAO-B inhibition by reference compounds *R*-(-)-deprenyl (0.16 μM), safinamide (0.12 μM) and the tested compound **12** (0.22 μM). The residual activity of undialysis and dialysis groups were expressed as % of control. Data were shown as mean ± SD of three independent experiments.

Introducing -Cl to C-5 position on the thienyl ring of **3** led to the most potent compound (**12**) among this class of inhibitors. Compound **12** exhibited an excellent inhibitory activity on *h*MAO-B with an $IC_{50}$ value of 0.11 μM, which was 118 and 5.5-fold more potent than chalcone and compound **3**. Introduction of 5-Br to the same position on the thienyl ring also significantly increased the inhibitory activity. The resulted compound (**13**) exhibited a comparable inhibitory activity with **12** ($IC_{50}$ = 0.12 μM). When introducing -$CH_3$ to the same position, the inhibitory activity of the resulted compound **14** increased by 2.2-fold compared to **3**, while 2.45-fold less potent than **12**. Thus, we concluded that substitution on the C-5 position on the thienyl ring of **3** would increase the inhibitory activity and the halogen atoms are preferable.

For the potent compound **12**, replacing the 1, 4-benzodioxan moiety with the 1, 3-dioxaindane (**15**) led to a marked decrease in the inhibitory activity ($IC_{50}$ = 0.43 μM). When cleaving the 1, 4-dioxan ring of **12**, the resulting compound bearing the 3, 4-dimethoxyphenyl (**16**) also showed very weak inhibition against *h*MAO-B (14.5% inhibition). Similarly, as for the compounds with reasonable inhibitory activities (**13**–**14**), replacing the 1, 4-benzodioxan moiety with the 1, 3-dioxaindane (**17**) or the methoxyphenyl moieties (**18**–**19**) led to much lower inhibitory activities (**17**, $IC_{50}$ = 0.80 μM; **18**, 12.3% inhibition; **19**, 28.2% inhibition) compared to the corresponding compounds. Together with the fact that the furan or pyrrole-substituted chalcone compounds with the methoxyphenyl moiety (**20**–**22**) had little inhibition against *h*MAO-B (< 5% inhibition), these results reinforce that the 1, 4-benzodioxan moiety is crucial for the inhibitory activity of this class of inhibitors.

An overview of the SAR of the 1, 4-benzodioxan-substituted thienyl chalcone compounds with respect to *h*MAO-B inhibition is provided in Fig. 4.

As for the *h*MAO-A, all the tested chalcone compounds showed less than 50% inhibition even at 40 μM. According the definition of selectivity index (SI), the most potent *h*MAO-B inhibitor **12** exhibited an SI value of greater than 363. Thus, we conclude that the potent inhibitors found in the current work are highly selective *h*MAO-B inhibitors.

## Kinetics study

To investigate the inhibiting mode by the active compounds, the most potent compound **12** was selected as a representative *h*MAO-B inhibitor and subjected to enzyme kinetic study. The Lineweaver–Burk graph was constructed in the absence or presence of inhibitors at various concentrations. As illustrated in Fig. 5A, the graphs of compound **12** in different concentrations were linear and intersect at the y-axis, which suggested that compound **12** is a competitive *h*MAO-B inhibitor.

## Reversibility study

To investigate whether the active compounds were irreversible or reversible *h*MAO-B inhibitors, the dialysis assay was conducted. The irreversible inhibitor *R*-(-)-deprenyl and the reversible inhibitor safinamide were used

as reference compounds. The most potent compound **12** was selected as a representative *h*MAO-B inhibitor. All the tested inhibitors were evaluated under the same experimental conditions.

In the dialysis assay, MAO-B was incubated with the tested inhibitors for 15 min and subsequently dialyzed for 24 h. As illustrated in Fig. 5B, after dialysis, the enzymatic activity of *R*-(-)-deprenyl treated group was hardly recovered with the residual activity of 16.3% of the control, which was comparable to that of the undialysis group (10.3%). While the enzymatic activity of the safinamide treated group was recovered from 47.1 to 90.6% after dialysis. Similar changes were observed for the compound **12** treated group, the enzymatic activity of which was recovered from 34.0 to 98.9% of the control after dialysis. These results distinctly showed that compound **12** was a reversible *h*MAO-B inhibitor.

## Molecular Docking studies

To investigate the possible interaction mechanism between the active compounds and *h*MAO-B, we performed a molecular docking study using the docking module in the software MOE. The co-crystal structure of *h*MAO-B was employed and the compounds were docked into the active site.

The *h*MAO-B active site consists of two cavities, the substrate cavity in front of the FAD and the entrance cavity located underneath the protein surface and closed by the loop formed by residues 99–112[26]. As shown in Fig. 6A, parent chalcone compound **1** adopted an extended pose in the active site of *h*MAO-B. The A ring occupied the hydrophobic pocket in the entrance cavity and the B ring was directed towards the substrate cavity. Compounds **2** and **3** adopted similar docking poses in the active site of *h*MAO-B. The thienyl ring of both compounds occupied the entrance cavity, whereas the 1, 4-benzodioxan moiety of **3** extended more deeply into the substrate cavity in front of FAD, which might strengthen the binding contact with the enzyme and consequently lead to increased inhibitory activity. As for the active compound **12**, the thienyl and 1, 4-benzodioxan moieties were located at the similar positions with **3** in the cavity. Besides, the 5′-Cl of this compound was embedded in a relative polar sub-pocket composed of Leu164, Ala 165 Leu167, Phe168 and formed a halogen bond with the

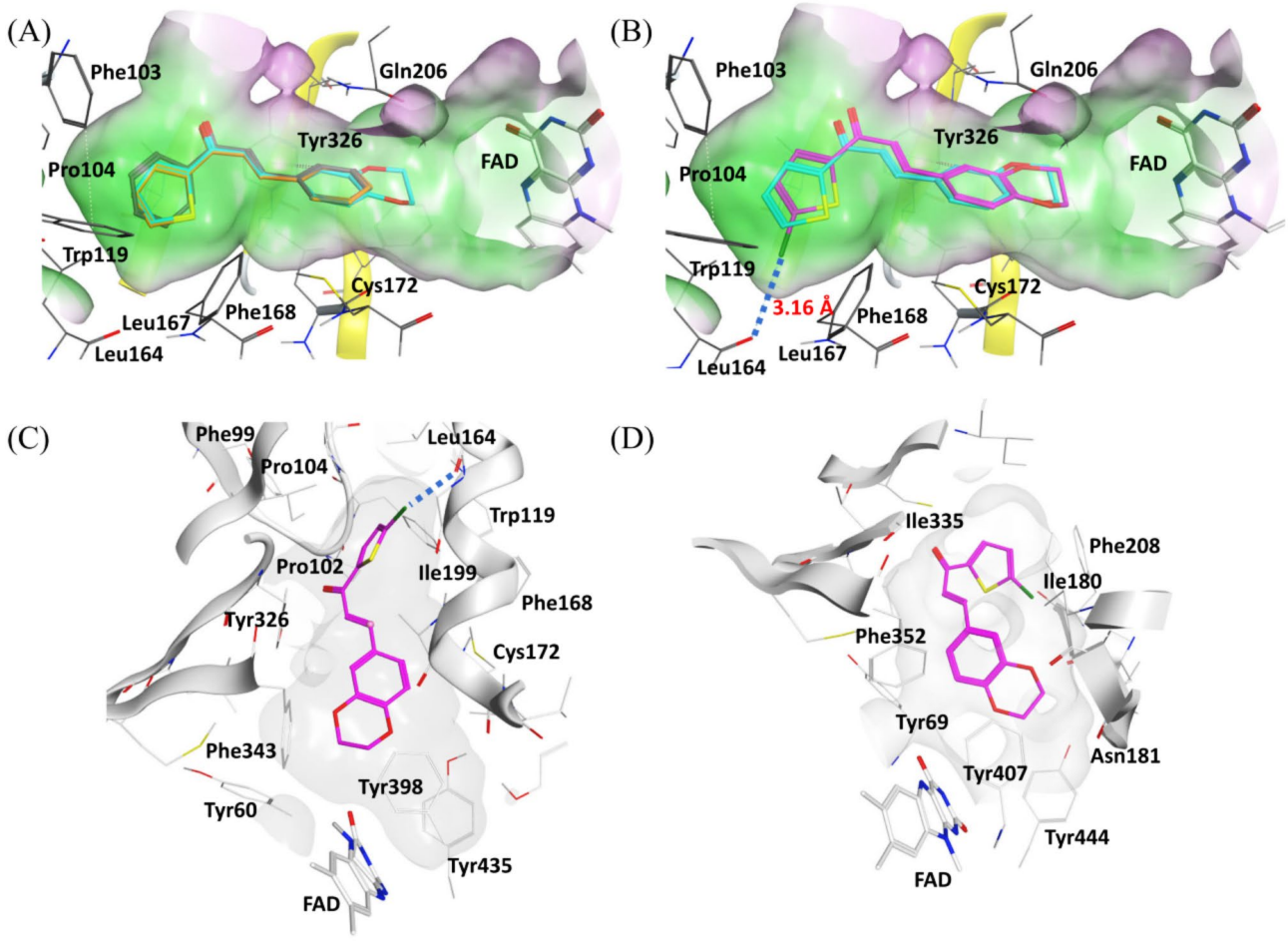


**Fig. 6**. (**A**) The docking results of compounds **1**, **2** and **3** within the active site of *h*MAO-B; (**B**) The docking results of compounds **3** and **12** within the active site of *h*MAO-B; (**C**) The docking result of compound **12** within the active site of *h*MAO-B; (**D**) The docking result of compound **12** within the active site of *h*MAO-A. Gray, compound **1**; brown, compound **2**; cyan, compound **3**; pink, compound **12**; blue dotted lines: halogen bond.

carbonyl oxygen of Leu164 (Fig. 6B-C) with a bond distance of 3.16 Å, which might play an important role in reinforcing the binding with the enzyme and lead to its higher inhibitory activity than other compounds. Another active compound **13** also adopted a similar docking pose with **12** and the 5′-Br formed a halogen bond with the carbonyl oxygen of Leu164 with a bond distance of 3.38 Å (**Fig.S1** in Supplementary Information).

To explain why the active compounds exhibited weak inhibitory activities against *h*MAO-A, compound **12** was selected as a case study in this series and docked into the active site of *h*MAO-A. It was found that the binding free energy of **12** with *h*MAO-A was much higher than that with *h*MAO-B (−5.7749 kcal/mol versus −7.994 kcal/mol, **Table S1** in Supplementary Information), which indicated that **12** had a lower binding affinity with *h*MAO-A. As illustrated in Fig. 6D, in contrast to its extended pose in binding with *h*MAO-B, **12** adopted a folded pose in the active site of *h*MAO-A. The 1, 4-benzodioxan moiety of this compound was located at the proximity of the FAD and the thienyl moiety pointed to the opposite side with a twisted chain of α, β-unsaturated ketone. The resulting folded pose might be due to the fact that *h*MAO-A has a single and shorter substrate cavity than *h*MAO-B[31], so that **12** adopted a folded conformation in order to avoid structural conflicts with the bulky side chains of surrounding residues such as Tyr69, Phe208 and Phe352. Yet the folded conformation of **12** would result in less productive interactions with *h*MAO-A, which had been observed in other large *h*MAO-B selective inhibitors[32]. As other active compounds (**3**, **13**–**14**) also exhibited lower binding free energy with *h*MAO-A compared to that with *h*MAO-B (**Table S1** in Supplementary Information), we hypothesis that steric hindrance might play a critical role in preventing these active compounds from binding to *h*MAO-A.

## ELISA

To investigate the anti-neuroinflammatory effect of compound **12**, the inhibitory effects of **12** on the production of pro-inflamatory mediators were then evaluated. The levels of NO, TNF-α and IL-1β were measured in or $A\beta_{1-42}$ - stimulated BV2 cells when treating with or without the tested compound.

As illustrated in Fig. 7A-C, LPS induced obvious release of the pro-inflammatory mediators from BV2 cells. The level of NO, TNF-α and IL-1β were evaluated up to 11.4-fold, 26.3-fold and 30.4-fold respectively compared to the control group. While pre-treating the cells with **12** at the concentrations of 1 and 10 μM for 6 h, the level of NO, TNF-α and IL-1β were then reduced in a dose-dependent manner in the LPS- stimulated cells, of which about 22.3–35.6%, 35.4–42.1% and 37.6–52.7% reduction in the release of NO, TNF-α and IL-1β, respectively, were observed at various concentrations of **12**.

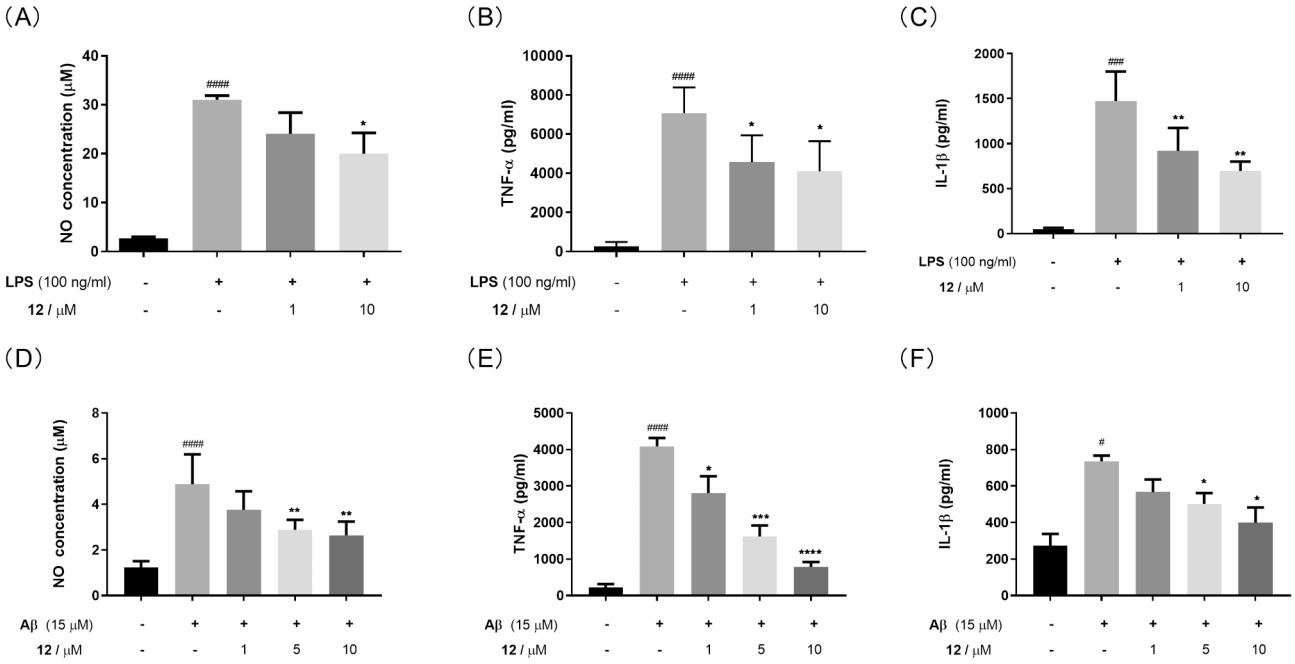


**Fig. 7**. Compound **12** inhibited the release of NO, TNF-α and IL-1β in LPS- and $A\beta_{1-42}$-stimulated BV2 cells. (**A**) The inhibitory effects of compound **12** on the release of NO in LPS-stimulated BV2 cells; (**B**) The inhibitory effects of compound **12** on the release of TNF-α in LPS-stimulated BV2 cells; (**C**) The inhibitory effects of compound **12** on the release of IL-β in LPS-stimulated BV2 cells; (**D**) The inhibitory effects of compound **12** on the release of NO in $A\beta_{1-42}$-stimulated BV2 cells; (**E**) The inhibitory effects of compound **12** on the release of TNF-α in $A\beta_{1-42}$-stimulated BV2 cells; (**F**) The inhibitory effects of compound **12** on the release of IL-β in $A\beta_{1-42}$-stimulated BV2 cells. The data are presented as mean ± SD of at least three independent experiments. Significant differences are shown using Student's *t*-test analysis. $^{*}p<0.05$, $^{**}p<0.01$, $^{***}p<0.001$, $^{****}p<0.0001$ versus the cells treated with LPS or $A\beta_{1-42}$ alone; $\#p<0.05$, $\#\#p<0.01$, $\#\#\#p<0.001$, $\#\#\#\#p<0.0001$ versus the control group cells.

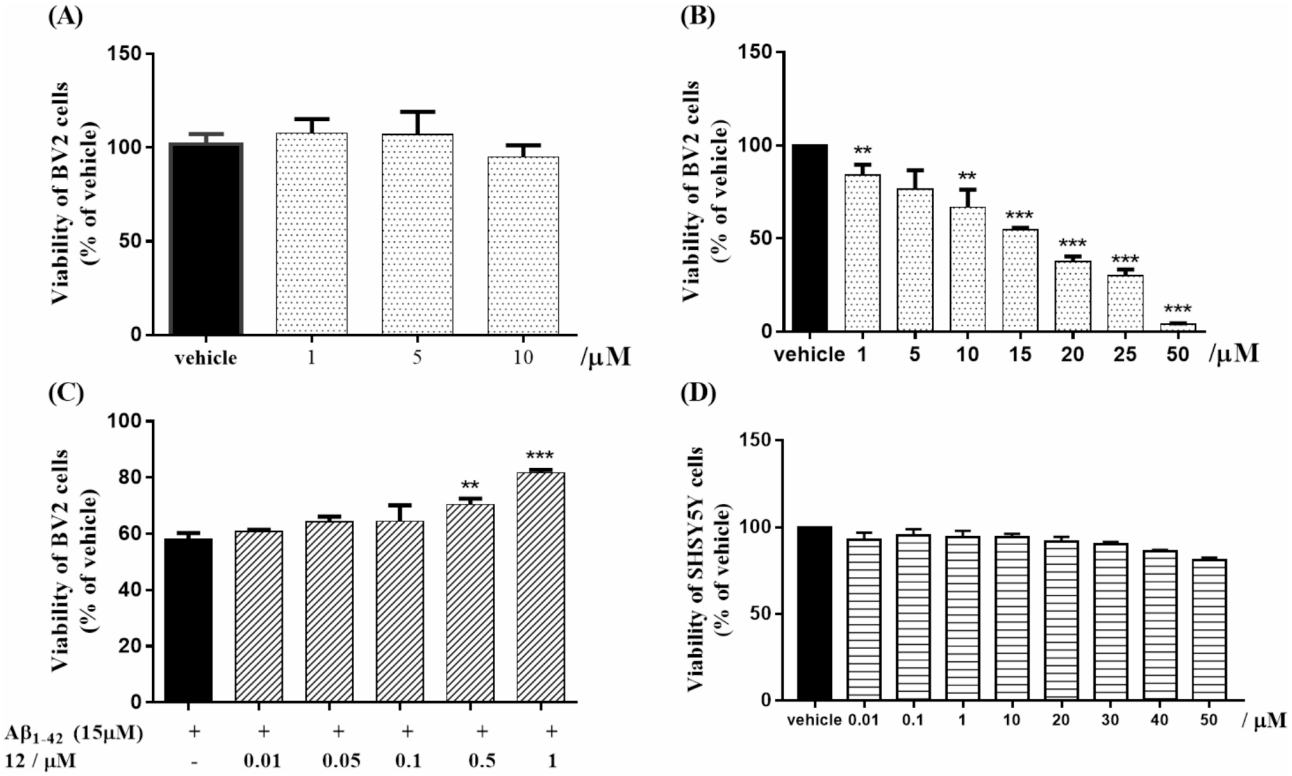


**Fig. 8**. (**A**) The cytotoxicity of compound **12** at various concentrations (1, 5 and 10 μM) towards BV2 cells; (**B**) The cytotoxicity induced by various concentrations of $A\beta_{1-42}$ (1–50 μM) in BV2 cells; (**C**) The viability of $A\beta_{1-42}$ (15 μM) treated BV2 cells after pre-treatment with compound **12** at different concentrations (0.01–1 μM). (**D**) The Cell viability of SHSY5Y cells after treatment with compound **12** at different concentrations (0.1–50 μM). Significant differences are shown using Student's *t*-test analysis. $^{**}p < 0.01$, $^{***}p < 0.001$ versus vehicle group cells or $A\beta_{1-42}$ -treated group cells.

We also investigated the inhibitory effects of compound **12** on the production of pro-inflammatory mediators in $A\beta_{1-42}$-stimulated BV2 cells. As illustrated in **Fig. 7D-F**, $A\beta_{1-42}$ induced about 4-fold, 18.5-fold and 2.7-fold increase on the level of NO, TNF-α and IL-1β respectively. While pre-treatment the cells with **12** at the concentrations of 1, 5 and 10 μM for 6 h, the level of NO, TNF-α and IL-1β in BV2 cells were reduced in a dose-dependent manner in the $A\beta_{1-42}$-stimulated cells, of which about 22.9 −46%, 31.3 −80.8% and 22.9 −45.6% reduction in the release of NO, TNF-α and IL-1β, respectively, were observed at various concentrations of **12**.

The above results suggested that the hit compound **12** could effectively inhibit the release of NO, TNF-α and IL-1β in both LPS- and $A\beta_{1-42}$-stimulated BV2 cells, which indicates its potential to be developed as an anti-neuroinflammation agent.

### MTT assay

To evaluate the neuroprotective effect of the potent compound **12**, MTT assay was performed to evaluate the cell viability in the presence of $A\beta_{1-42}$ with or without the tested compound. First, the cytotoxicity of compound **12** was determined in BV2 cells. As illustrated in Figs. 8A and 12 exhibited little cytotoxicity in BV2 cells at the tested concerntrations (1–10 μM). We then investigated the cytotoxicity induced by various concentrations of $A\beta_{1-2}$ in BV2 cells. The results showed that $A\beta_{1-42}$ reduced the cell viability in a dose dependent manner, of which the percentage of viable cells was 57.1% compared to vehicle at 15 μM (Fig. 8B). But when pre-treatment with compound **12** at 0.01–1 μM for 24 h, the cell viability was recovered by 3–24% compared to the $A\beta_{1-42}$-treated group (Fig. 8C). These results suggest that **12** could attenuate the cytotoxicity induced by $A\beta_{1-42}$ in BV-2 cells. Taking account of the fact that **12** exhibit little cytotoxicity in SHSY5Y cells (0.01–50 μM, Fig. 8D), we suppose the potent compound could be developed as a potential neuroprotective agent with a wide safety window.

## Conclusion

In this study, we reported the development of a series of 1, 4-benzodioxan-substituted thienyl chalcone derivatives that serve as novel MAO-B reversible inhibitors. The SAR study highlighted the importance of the thienyl and 1, 4-benzodioxan moieties on inhibiting MAO-B. And the presence of 5'-Cl at the thienyl ring significantly enhanced the inhibitory potency. The most potent compound **12** exhibited an $IC_{50}$ value of 0.11 μM with an SI value greater than 363. Kinetics and reversibility studies confirmed that compound **12** acted as a competitive and reversible inhibitor of *h*MAO-B. Computational docking studies further provided insights into the interaction between active compounds and the enzyme. Moreover, **12** displayed significant inhibitory effects on the releases

of pro-inflammatory mediators NO, TNF-α and IL-1β in the LPS or $A\beta_{1-42}$-stimulated BV2 cells, while also attenuating the cytotoxicity induced by $A\beta_{1-42}$ in BV2 cells. In conclusion, our findings present an opportunity for the discovery of novel potent MAO-B inhibitors that also possess anti-neuroinflammatory activity.

## Data availability

The datasets used and analysed during the current study available from the corresponding author on reasonable request.

Received: 10 October 2024; Accepted: 4 March 2025
Published online: 13 March 2025

## References

1. Barnham, K. J., Masters, C. L. & Bush, A. I. Neurodegenerative diseases and oxidative stress. *Nat. Rev. Drug Discovery*. **3** (3), 205–214. https://doi.org/10.1038/nrd1330 (2004).
2. Zhang, W., Xiao, D., Mao, Q. & Xia, H. Role of neuroinflammation in neurodegeneration development. *Signal. Transduct. Target. Therapy*. **8** (1), 267. https://doi.org/10.1038/s41392-023-01486-5 (2023).
3. Niveta, J. P. S., John, C. M. & Arockiasamy, S. Monoamine oxidase mediated oxidative stress: a potential molecular and biochemical crux in the pathogenesis of obesity. *Mol. Biol. Rep.* **51** (1), 29. https://doi.org/10.1007/s11033-023-08938-9 (2023).
4. Santin, Y., Resta, J., Parini, A. & Mialet-Perez, J. Monoamine oxidases in age-associated diseases: new perspectives for old enzymes. *Ageing Res. Rev.* **66**, 101256. https://doi.org/10.1016/j.arr.2021.101256 (2021).
5. Jones, D. N. & Raghanti, M. A. The role of monoamine oxidase enzymes in the pathophysiology of neurological disorders. *J. Chem. Neuroanat.* **114**, 101957. https://doi.org/10.1016/j.jchemneu.2021.101957 (2021).
6. Ramsay, R. R. Molecular aspects of monoamine oxidase B. Progress in Neuro-Psychopharmacology and biological psychiatry. ;**69**:81–89. (2016). https://doi.org/10.1016/j.pnpbp.2016.02.005
7. Youdim, M. B. H. & Bakhle, Y. S. Monoamine oxidase: isoforms and inhibitors in Parkinson's disease and depressive illness. *Br. J. Pharmacol.* **147** (S1), S287–S96. https://doi.org/10.1038/sj.bjp.0706464 (2006).
8. Saura, J. et al. Increased monoamine oxidase B activity in plaque-associated astrocytes of alzheimer brains revealed by quantitative enzyme radioautography. *Neuroscience* **62** (1), 15–30. https://doi.org/10.1016/0306-4522(94)90311-5 (1994).
9. Manzoor, S. & Hoda, N. A comprehensive review of monoamine oxidase inhibitors as Anti-Alzheimer's disease agents: A review. *Eur. J. Med. Chem.* **206**, 112787. https://doi.org/10.1016/j.ejmech.2020.112787 (2020).
10. Youdim, M. B. H., Edmondson, D. & Tipton, K. F. The therapeutic potential of monoamine oxidase inhibitors. *Nat. Rev. Neurosci.* **7** (4), 295–309. https://doi.org/10.1038/nrn1883 (2006).
11. Carradori, S. & Silvestri, R. New frontiers in selective human MAO-B inhibitors. *J. Med. Chem.* **58** (17), 6717–6732. https://doi.org/10.1021/jm501690r (2015).
12. de Araújo Boleti, A. P. et al. An overview of neurodegenerative and metabolic diseases and of biotechnological studies. *Neurochem. Int.* **136**, 104714. https://doi.org/10.1016/j.neuint.2020.104714 (2020).
13. Heneka, M. T. et al. Neuroinflammation in Alzheimer's disease. *Lancet Neurol.* **14** (4), 388–405. https://doi.org/10.1016/S1474-4422(15)70016-5 (2015).
14. Leng, F. & Edison, P. Neuroinflammation and microglial activation in alzheimer disease: where do we go from here? *Nat. Reviews Neurol.* **17** (3), 157–172. https://doi.org/10.1038/s41582-020-00435-y (2021).
15. Gao, C., Jiang, J., Tan, Y. & Chen, S. Microglia in neurodegenerative diseases: mechanism and potential therapeutic targets. *Signal. Transduct. Target. Therapy*. **8** (1), 359. https://doi.org/10.1038/s41392-023-01588-0 (2023).
16. Guglielmi, P., Mathew, B., Secci, D., Carradori, S. & Chalcones Unearthing their therapeutic possibility as monoamine oxidase B inhibitors. *Eur. J. Med. Chem.* **205**, 112650. https://doi.org/10.1016/j.ejmech.2020.112650 (2020).
17. Chimenti, F. et al. Chalcones: a valid scaffold for monoamine oxidases inhibitors. *J. Med. Chem.* **52** (9), 2818–2824. https://doi.org/10.1021/jm801590u (2009).
18. Parambi, D. G. T. et al. Design, synthesis and biological evaluation of oxygenated Chalcones as potent and selective MAO-B inhibitors. *Bioorg. Chem.* **93**, 103335. https://doi.org/10.1016/j.bioorg.2019.103335 (2019).
19. Minders, C., Petzer, J. P., Petzer, A. & Lourens, A. C. Monoamine oxidase inhibitory activities of heterocyclic Chalcones. *Bioorg. Med. Chem. Lett.* **25** (22), 5270–5276. https://doi.org/10.1016/j.bmcl.2015.09.049 (2015).
20. Mathew, B. et al. Exploration of chlorinated Thienyl Chalcones: A new class of monoamine oxidase-B inhibitors. *Int. J. Biol. Macromol.* **91**, 680–695. https://doi.org/10.1016/j.ijbiomac.2016.05.110 (2016).
21. Wu, J. et al. Evaluation and discovery of novel synthetic chalcone derivatives as Anti-Inflammatory agents. *J. Med. Chem.* **54** (23), 8110–8123. https://doi.org/10.1021/jm200946h (2011).
22. Kong, Z., Sun, D., Jiang, Y. & Hu, Y. Design, synthesis, and evaluation of 1, 4-benzodioxan-substituted Chalcones as selective and reversible inhibitors of human monoamine oxidase B. *J. Enzyme Inhib. Med. Chem.* **35** (1), 1513–1523. https://doi.org/10.1080/14756366.2020.1797711 (2020).
23. Lu, C. et al. Design, synthesis, and evaluation of Multitarget-Directed Resveratrol derivatives for the treatment of Alzheimer's disease. *J. Med. Chem.* **56** (14), 5843–5859. https://doi.org/10.1021/jm400567s (2013).
24. Sun, D. et al. Benzodioxane Carboxamide derivatives as novel monoamine oxidase B inhibitors with antineuroinflammatory activity. *ACS Med. Chem. Lett.* **15** (6), 798–805. https://doi.org/10.1021/acsmedchemlett.3c00532 (2024).
25. Mostert, S., Petzer, A. & Petzer, J. P. The evaluation of 1,4-benzoquinones as inhibitors of human monoamine oxidase. *Eur. J. Med. Chem.* **135**, 196–203. https://doi.org/10.1016/j.ejmech.2017.04.055 (2017).
26. Binda, C. et al. Structures of human monoamine oxidase B complexes with selective noncovalent inhibitors: Safinamide and coumarin analogs. *J. Med. Chem.* **50** (23), 5848–5852. https://doi.org/10.1021/jm070677y (2007).
27. Son, S-Y. et al. Structure of human monoamine oxidase A at 2.2-Å resolution: The control of opening the entry for substrates/inhibitors. Proceedings of the National Academy of Sciences. ;105(15):5739-44. (2008). https://doi.org/10.1073/pnas.0710626105
28. Distinto, S. et al. Synthesis and biological assessment of novel 2-thiazolylhydrazones and computational analysis of their recognition by monoamine oxidase B. *Eur. J. Med. Chem.* **48**, 284–295. https://doi.org/10.1016/j.ejmech.2011.12.027 (2012).
29. Fang, Y. et al. Design, synthesis, and biological evaluation of compounds with a new scaffold as anti-neuroinflammatory agents for the treatment of Alzheimer's disease. *Eur. J. Med. Chem.* **149**, 129–138. https://doi.org/10.1016/j.ejmech.2018.02.063 (2018).
30. Li, Y. et al. Multitarget drug design strategy against Alzheimer's disease: homoisoflavonoid Mannich base derivatives serve as acetylcholinesterase and monoamine oxidase B dual inhibitors with multifunctional properties. *Bioorg. Med. Chem.* **25** (2), 714–726. https://doi.org/10.1016/j.bmc.2016.11.048 (2017).
31. De Colibus, L. et al. Three-dimensional structure of human monoamine oxidase A (MAO A): relation to the structures of rat MAO A and human MAO B. *Proc. Natl. Acad. Sci.* **102** (36), 12684–12689. https://doi.org/10.1073/pnas.0505975102 (2005).
32. Legoabe, L. J., Petzer, A. & Petzer, J. P. Selected C7-substituted Chromone derivatives as monoamine oxidase inhibitors. *Bioorg. Chem.* **45**, 1–11. https://doi.org/10.1016/j.bioorg.2012.08.003 (2012).

## Author contributions

All authors contributed to the study conception and design. All authors read and approved the final manuscript. The synthesis and identification of compounds were performed by Demeng Sun and Zuo Kong. The assays of biological evaluation were performed by Demeng Sun, Yanmei Jiang, Bo Wang and Mengxue Mu. The X-ray diffraction analysis was performed by Jingbo Tan. The molecular modelling analysis was performed by Yun Hu. The original draft of the manuscript was written by Yun Hu.

## Funding

This work was supported by the National Natural Science Foundation of China under Grant [No. 81560562 and 21762055] and the Science and Technology Department of Guizhou Province under grant (QKHJC-ZK[2024] YB288).

## Declarations

## Competing interests

The authors declare no competing interests.

## Additional information

**Supplementary Information** The online version contains supplementary material available at https://doi.org/10.1038/s41598-025-93076-4.

**Correspondence** and requests for materials should be addressed to Y.H.

**Reprints and permissions information** is available at www.nature.com/reprints.

**Publisher's note** Springer Nature remains neutral with regard to jurisdictional claims in published maps and institutional affiliations.